J5.7 FEFLO CFD MODEL STUDY OF FLOW AND DISPERSION AS INFLUENCED BY TALL BUILDINGS IN NEW YORK CITY

Fernando E. Camelli[1*], Steven R. Hanna[2], and Rainald Löhner[1]

[1]Laboratory for Computational Fluid Dynamics
School of Computational Sciences
George Mason University, Fairfax, Virginia
[2]Hanna Consultants
Kennebunkport, Maine

1. INTRODUCTION

This paper studies flow and dispersion patterns in Manhattan using the multipurpose finite element code FEFLO-URBAN. The computational domain is 3.2 km in the East-West direction, and 2.6 km in the South-North direction. This study was conducted as part of a collaborative effort with several agencies to support a field experiment carried out in the Madison Square Garden (MSG) area in March, 2005. Three other Computational Fluid Dynamics (CFD) models also participated in this collaboration - Fluent (EPA), CFD-Urban (CFD Research), and FLACS (GexCon). With FEFLO-URBAN, a very large eddy simulation (VLES) model was used to simulate wind and dispersion conditions. First, as part of the planning exercise, five continuous releases from points at street level around Madison Square Garden with winds from the South-West were simulated. Then, a wind from the West-North-West was simulated to represent the actual conditions found during the field experiment. For this last wind condition, five continuous and five puff releases were simulated. A tetrahedral mesh of 24 million elements was used for this study. A resolution of approximately 1 meter was set at the street level and close to walls. A logarithmic wind profile was assumed as the inflow boundary condition, assuming the observed wind speed of about 5 m/s at a height of about 200 m. The simple Smagorinsky turbulence model was used as closure to the filtered flow equations. An explicit integration in time was used to capture the unsteady patterns of the flow. A time period of 1,000 seconds was integrated for the SW wind, and 1,500 seconds for the WNW wind. Profiles of turbulent kinetic energy (TKE), as well as concentration levels, were extracted at selected locations. A qualitative study of flow and dispersion patterns around the Madison Square Garden is presented in this paper. The study includes the enhancement of the plume's width related to the wind direction with respect to the street direction, and the resulting chimney effects behind the surrounding tall buildings.

[*] *Corresponding author address*: Fernando E. Camelli, CFD Lab, MS 4C7, School of Computational Sciences, George Mason University, Fairfax, VA 22030;
e-mail: fcamelli@gmu.edu

2. MODEL DESCRIPTION

Atmospheric flow is mathematically modeled by the unsteady incompressible Navier-Stokes equations in 3D. Numerical solutions for these equations are obtained using FEFLO-URBAN, a multi-purpose finite element (Löhner 1990). The code is based on the following general principles: use of unstructured grids (automatic grid generation and mesh refinement); finite element discretization of space; and edge-based data structures for computational speed. The two most common types of grids used in the code for CFD simulations are body-conforming and embedded grids. For body-conforming grids the external mesh faces match up with the surface (building surfaces) of the domain. In the embedded approach (also known as fictitious domain, or immersed boundary), the surface is placed inside a large mesh with special treatment of the elements close to the surface (Löhner et al. 2004). For large cities where many buildings are present the later approach is used for simplicity.

FEFLO can operate in two levels of approximation: Reynolds Averaged Navier-Stokes (RANS) and very large eddy simulation (VLES). The Navier-Stokes equations are time filtered in RANS and space filtered in VLES. FEFLO-Urban is used in VLES mode. The filtered equations are close with the Smagorinsky model (Smagorinsky 1963). The inflow boundary condition for VLES simulations usually is unsteady, and in FEFLO is reproduced synthetically (Hanna et al. 2002). The present runs were performed without unsteady inflow.

FEFLO-Urban has been validated against field experiments (Camelli; Löhner 2000b; Camelli et al. 2004a) and wind-tunnel experiments (Camelli; Löhner 2000a; Camelli et al. 2004b; Hanna et al. 2002).

2.1 *Time Integration*

An explicit integration in time for the advective terms was used to capture the unsteadiness of the flow around the containers. Most of the diffusion in the atmosphere is due to the turbulent nature of the flow. The molecular diffusion is usually two orders of magnitude lower than the turbulent diffusion. Therefore, the time step selected for integration in time has to be small enough such that all the high frequencies that contribute to the turbulent diffusion are properly resolved in time.

2.2 *Projection Scheme*

The equations describing incompressible, Newtonian flows are written as

$$\frac{\partial \mathbf{v}}{\partial t} + \mathbf{v}\nabla\mathbf{v} + \nabla p = \nabla \nu \nabla \mathbf{v} \quad (1)$$

$$\nabla \cdot \mathbf{v} = 0 \quad (2)$$

Here *p* denotes the pressure normalized by the constant density ρ, **v** the velocity vector and ν kinematic viscosity. The important physical phenomena propagate with the advective timescales, i.e. with **v**. Diffusive phenomena typically occur at a much faster rate, and can/should therefore be integrated implicitly. Given that the pressure establishes itself immediately through the pressure-Poisson equation, an implicit integration of pressure is also required. The hyperbolic character of the advection operator and the elliptic character of the pressure-Poisson equation have led to a number of so-called projection schemes. The key idea is to predict first a velocity field from the current flow variables without taking the divergence constraint into account. In a second step, the divergence constraint is being separated into an advective-diffusive and pressure increment:

$$\mathbf{v}^{n+1} = \mathbf{v}^{n} + \Delta\mathbf{v}^{a} + \Delta\mathbf{v}^{p} = \mathbf{v}^{*} + \Delta\mathbf{v}^{p} \quad (3)$$

For an explicit integration of the advective terms (with implicit integration of the viscous terms), one complete time-step is given by:

– Advective-Diffusive Prediction: $\mathbf{v}^{n} \rightarrow \mathbf{v}^{*}$

$$\left[\frac{1}{\Delta t} - \theta \nabla \nu \nabla\right]\left(\mathbf{v}^{*} - \mathbf{v}^{n}\right) + \mathbf{v}^{n} \cdot \nabla\mathbf{v}^{n} + \nabla p^{n} = \nabla \nu \nabla \mathbf{v}^{n} \quad (4)$$

– Pressure Correction: $p^{n} \rightarrow p^{n+1}$

$$\nabla \cdot \mathbf{v}^{n+1} = 0 \quad (5)$$

$$\frac{\mathbf{v}^{n+1} - \mathbf{v}^{*}}{\Delta t} + \nabla\left(p^{n+1} - p^{n}\right) = 0 \quad (6)$$

which results in

$$\nabla^{2}\left(p^{n+1} - p^{n}\right) = \frac{\nabla \cdot \mathbf{v}^{*}}{\Delta t} \quad (7)$$

– Velocity Correction: $\mathbf{v}^{*} \rightarrow \mathbf{v}^{n+1}$

$$\mathbf{v}^{n+1} = \mathbf{v}^{*} - \Delta t \nabla\left(p^{n+1} - p^{n}\right) \quad (8)$$

At steady state, $\mathbf{v}^{*} = \mathbf{v}^{n} = \mathbf{v}^{n+1}$ and the residuals of the pressure correction vanish, implying that the results do not depend on the time-step Δt. θ denotes the implicitness-factor for the viscous terms (θ=1.0: 1st order, fully implicit, θ=0.5: 2nd order, Cranck-Nicholson). This scheme has been widely used in conjunction with spatial discretization based on finite differences (Alessandrini; Delhommeau 1996; Bell; Marcus 1992; Bell et al. 1989; Kim; Moin 1985), finite volumes (Kallinderis; Chen 1996), and finite elements (Eaton 2001; Karbon; Singh 2002; Löhner 1990; Löhner et al. 1999; Ramamurti; Löhner 1996).

2.3 *Multi-stage Explicit Advective Prediction Scheme*

The scheme given by Equations (4-8) is, at best, of 2nd order in time. It is surprising to note that apparently no attempt has been made to use multistage explicit schemes to integrate the advective terms with higher order or to accelerate the convergence to steady state. This may stem from the fact that the implicit integration of viscous terms apparently impedes taking the full advantage multistage schemes offer for the Euler limit of no viscosity. An interesting alternative, used here, is to integrate with different time-stepping schemes in the different regimes of flows with highly variable cell Reynolds-number

$$Re_h = \frac{\|\mathbf{v}\| h}{\nu} \tag{9}$$

For the case $Re_h < 1$ (viscous dominated), the accuracy in time is not important. However, for $Re_h > 1$ (advection dominated), the advantages of higher order time-marching schemes are considerable, particularly if one considers vortex transport over large distances. Dahlquist's theorem states that no unconditionally stable (implicit) scheme can be of order higher than two (this being the Cranck-Nicholson scheme). However, explicit schemes of the Runge-Kutta type can easily yield higher order time stepping. A *k*-step, time-accurate Runge-Kutta scheme for the advective parts may be written as:

$$\begin{gathered} \mathbf{v}^i = \mathbf{v}^0 + \\ \alpha^i \gamma\left(-\mathbf{v}^{i-1} \cdot \nabla \mathbf{v}^{i-1} - \nabla p^n + \nabla \nu \nabla \mathbf{v}^{i-1}\right) \\ i = 1, k-1 \end{gathered} \tag{10}$$

$$\begin{gathered} \left[\frac{1}{\Delta t} - \theta \nabla \nu \nabla\right]\left(\mathbf{v}^k - \mathbf{v}^n\right) + \\ \mathbf{v}^{k-1} \cdot \nabla \mathbf{v}^{k-1} + \nabla p^n = \nabla \nu \nabla \mathbf{v}^{k-1}. \end{gathered} \tag{11}$$

Here, the α^i's are the standard Runge-Kutta coefficients, and θ is the implicitness-factor for the viscous terms (θ=1: 1st order, fully implicit, θ=0.5: 2nd order, Crank-Nicholson). The factor γ denotes the local ratio of the stability limit for explicit time stepping for the viscous terms versus the time-step chosen. Given that the advective and viscous time-step limits are proportional to:

$$\Delta t_a \approx \frac{h}{\|\mathbf{v}\|}; \Delta t_v \approx \frac{h^2}{\nu}; \tag{12}$$

we immediately obtain

$$\gamma = \min(1, Re_h). \tag{13}$$

In regions away from boundary layers, this factor is *O*(1), implying that a high-order Runge-Kutta scheme is recovered. Note that not using γ leads to schemes that are not of second order for the advective terms, unless an un-symmetric matrix is allowed on the left hand side. Besides higher accuracy, an important benefit of explicit multistage advection schemes is the larger time-step one can employ. The increase in allowable time-step is roughly proportional to the stages used. Given that most of the CPU time is spent solving the pressure-Poisson system (5), the speedup achieved is also roughly proportional to the stages used (Löhner 2004).

3. DESCRIPTION OF THE MADISON SQUARE GARDEN SIMULATION (MSG05)

A CFD simulation solves the Navier-Stokes equations in a computational domain. The computational domain is a geometrical representation of the objects present in the model. These objects are the buildings in the case of an urban simulation. The geometry of the buildings can be expressed as exact as the user wants and as the resolution of the tessellation of the domain allows. The geometrical representation of the buildings of an entire city usually takes many man hours. The commercial building database Vexcel was used to recover the geometry description of the city. This database was provided by Alan Huber from EPA under a collaboration effort to model the wind fields and dispersion patterns around Madison Square Garden. Figure 1 shows the blue print of the information contained in the database. A subset of the city was used in the present work (see Figure 2). The covering area of buildings included in the simulation is 2.7 km by 1.9 km. The computational domain is 3.3 km by 2.6 km and a height of 600 m. The buildings were model using the embedded approach (Löhner et al. 2004). This novel approach dramatically reduced the man-hours required for reconstructing the geometry of buildings as compared to the body-fitted approach.

Figure 1: New York City.

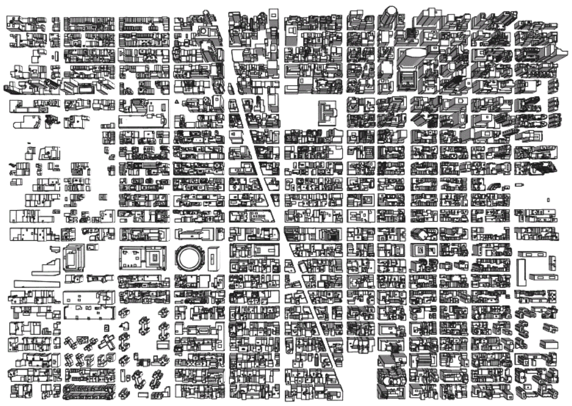

Figure 2: Aerial view of Madison Square Garden area.

Figure 3: Empire State Building.

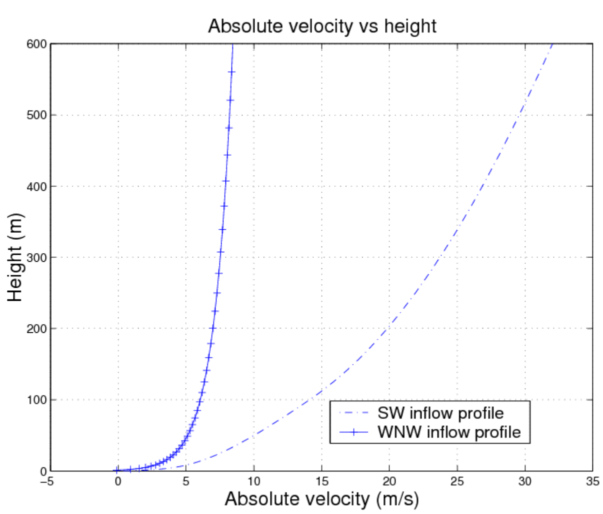

Figure 4: Logarithmic wind profile used in the SW and WNW simulations.

A VLES simulation was performed in a mesh of 24 millions of elements with an element size of 2 meters close to the building surfaces. Winds from the SW and the WNW directions were simulated. A logarithmic profile was imposed as a boundary condition in the inflow in each case (see Figure 4). The pressure was prescribed in the rest of the open boundaries and the velocity is free to change.

4. RESULTS FOR MSQ SIMULATIONS

4.1 *Wind Field Characterization*

The inflow conditions for the SW and WNW are dramatically different, from the direction to the wind velocity at 10 meters above ground level. These two simulations give very different patterns in the wind fields around the Madison Square Garden.

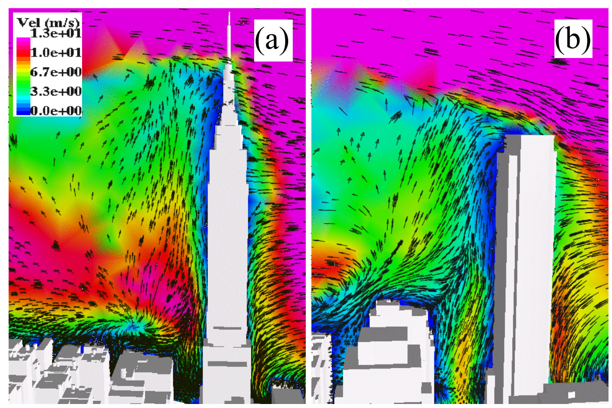

Figure 5: SW wind direction case. Empire State and One Penn Plaza Buildings

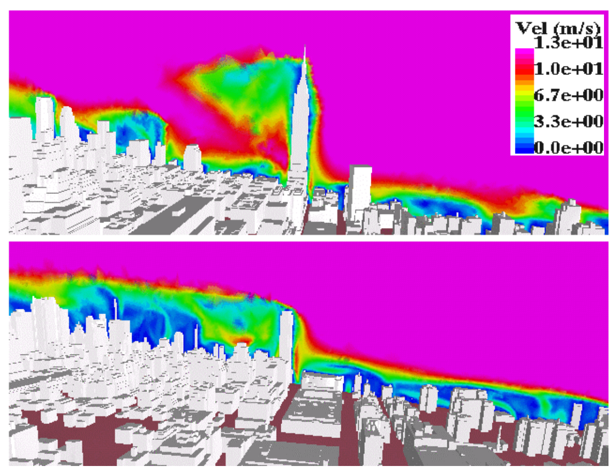

Figure 6: Air-wake behind Empire State and One Penn Plaza Buildings.

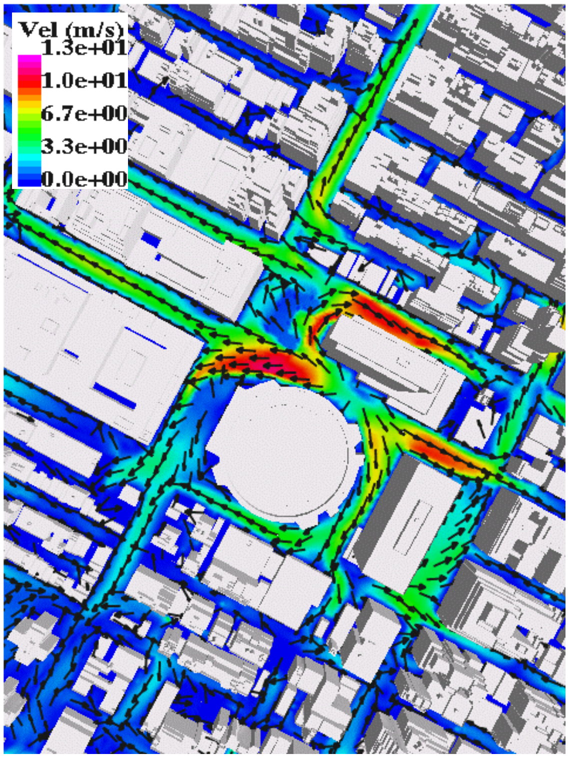

Figure 7: SW Case. Velocity vectors at 5 m above the ground level.

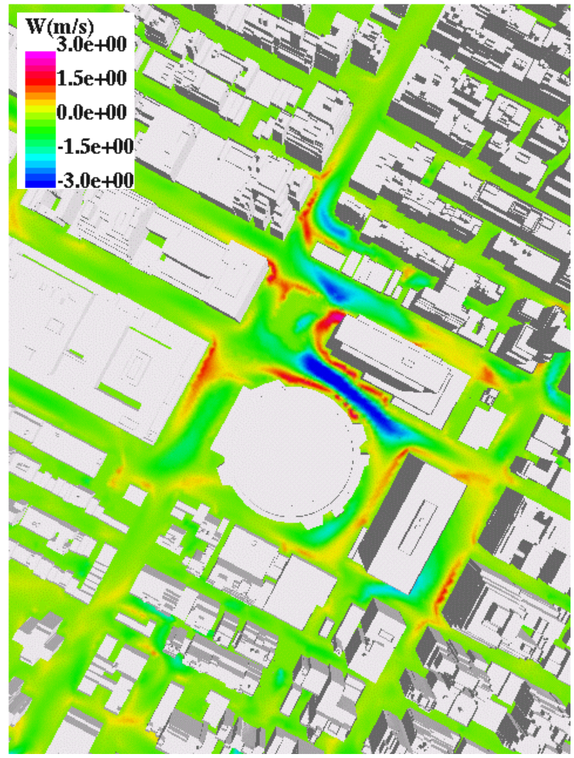

Figure 9: SW Case. Vertical velocity at 5 m above ground level.

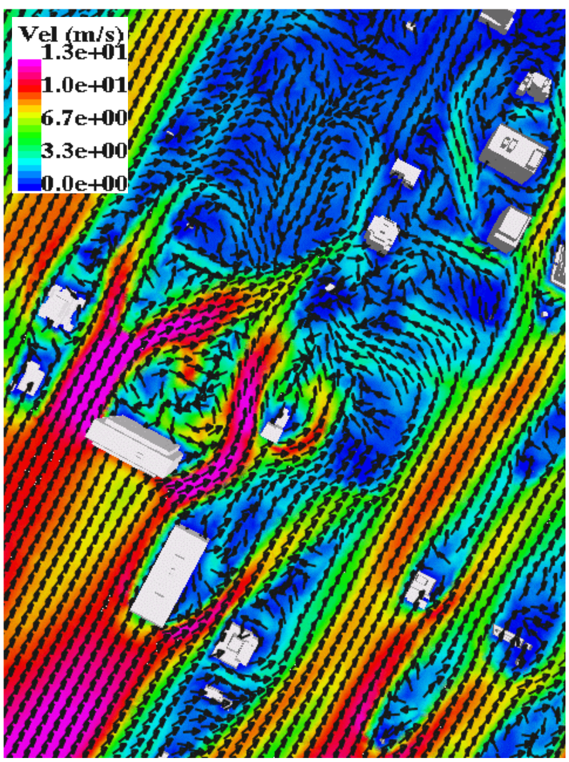

Figure 8: SW Case. Velocity vectors at 100 m above ground level.

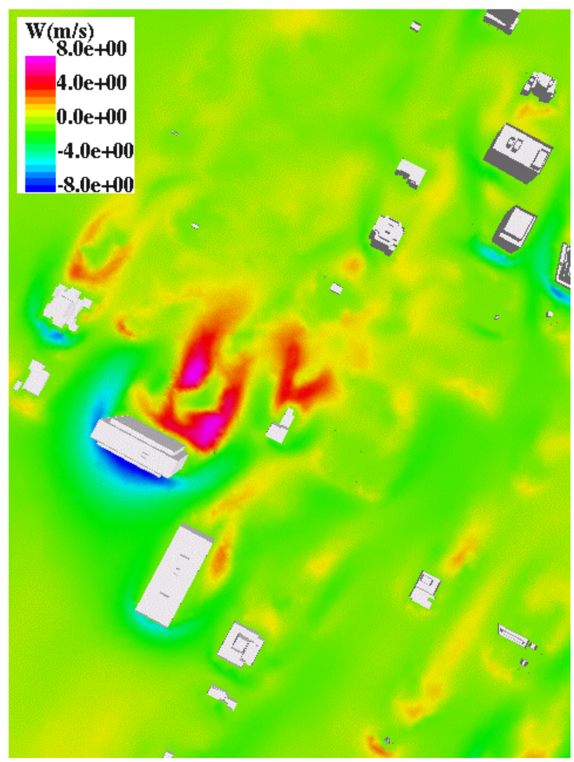

Figure 10: SW Case. Vertical velocity at 100 m above ground level.

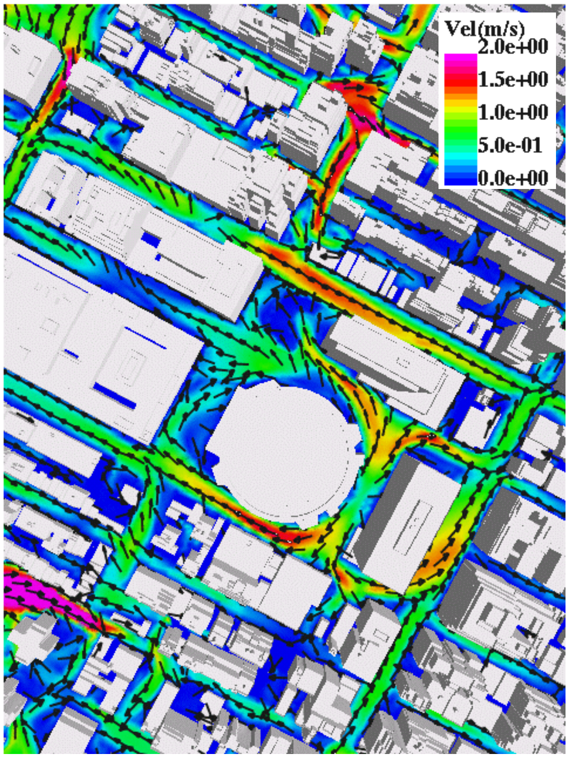

Figure 11: WNW Case. Velocity vectors at 5 m above the ground level.

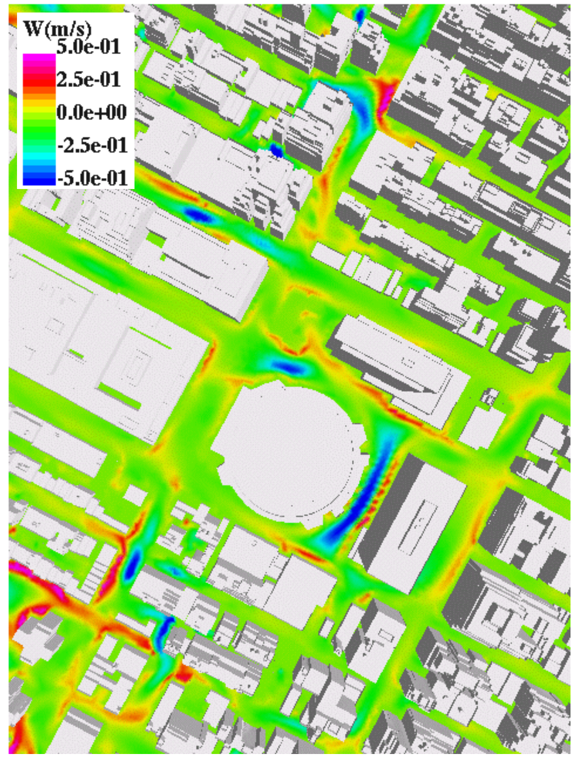

Figure 13: SW Case. Vertical velocity at 5 m above ground level.

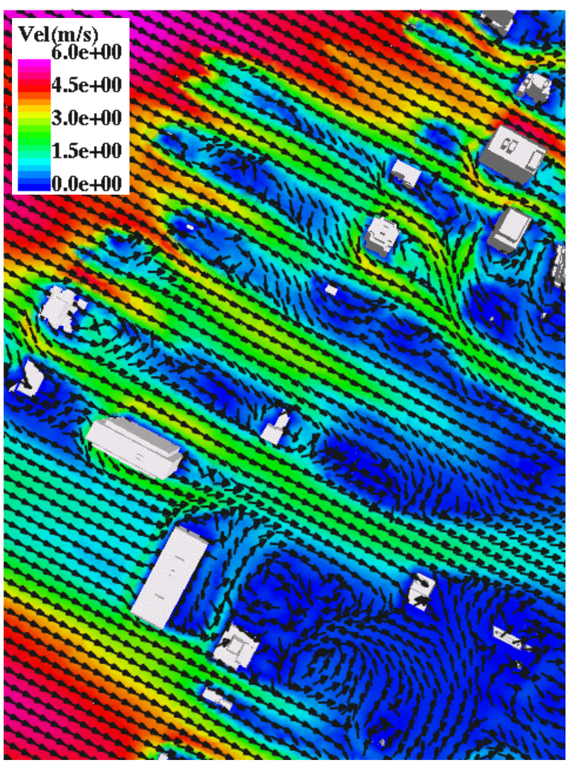

Figure 12: WNW Case. Velocity vectors at 100 m above ground level.

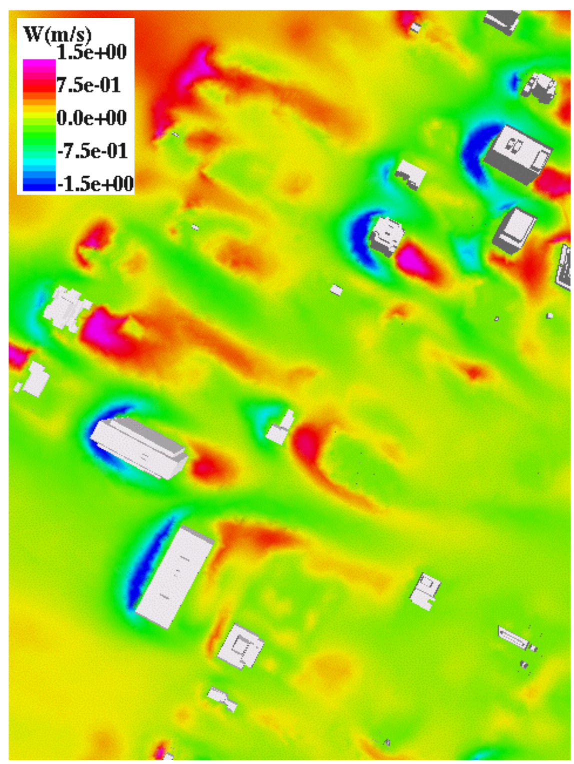

Figure 14: WNW Case. Vertical velocity at 100 m above ground level.

Figure 5 shows the velocity vectors in the wind direction plane for the Empire State building (a) and the One Penn Plaza building (b). Figure 5.a illustrates the air wake of the Empire State Building and the strong upward flow as a consequence of this tall building. The same effect is observed in the One Penn Plaza building. This upward current can be observed with any tall building. The flow field produces a chimney effect in the downwind face of the building.

Figure 6 shows the airwakes that are produced by the Empire State and One Penn Plaza buildings. The planes are in the inflow wind direction and they are colored with the absolute value of the velocity. The two airwakes are quite different. The airwake of the Empire State building is shorter in the down-wind direction than the airwake of the One Penn Plaza building. One possible explanation to this difference is the different density of tall buildings in the neighborhood of the Empire State. Although the Empire State is taller, there are few taller buildings surrounding it.

Figures 7 and 8 show the velocity vectors at 5 and 100 meters above ground level at the MSG area. The background color is the absolute value of the velocity. Velocities of the order of 10 m/s are observed around the One Penn Plaza at 5 meters above ground level. Figure 8 shows very complex eddies in the airwake of the tall buildings with areas of very low wind velocity. Figures 9 and 10 show the contour plot of the vertical velocity at 5 and 100 meters above ground level. Velocities of 2 m/s and -3 m/s are observed at the up-wind face of the One Penn Plaza. Figure 10 shows that the velocity is upward in the down-wind face of the buildings while is downward in the up-wind face of the building.

Figures 11 to 14 show the velocity vectors and contour plot of the vertical velocity for the WNW wind case.

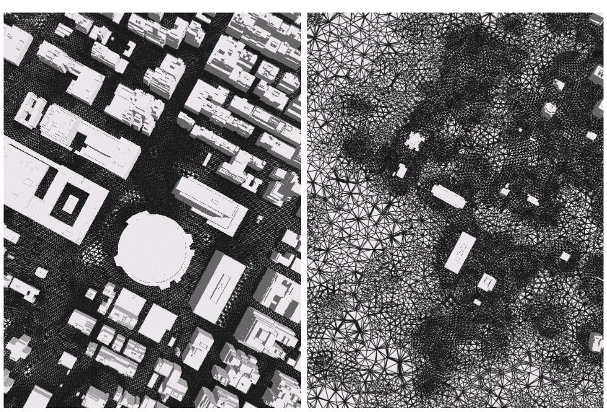

Figure 15: Cut mesh at 5 and 100 meters above ground level.

4.2 *Dispersion Patterns*

In the dispersion simulation, five near ground continuous releases were studied. Four releases were located at each corner of the MSG, and one at 34th Street in front of the One Penn Plaza. For the release with the SW wind, 1800 seconds were integrated; and for the WNW wind, 1000 seconds. The release rates were of 1 gram per second with the SW wind, and 130 grams per second with the WNW wind. Figure 16 shows the plume of the five releases for 10, 500 and 1000 seconds with the SW wind. The plane shown in Figure 10 is at 14 meters above ground level. The plume shows a large dispersion in the direction transversal to the wind. The One Penn Plaza produced a large recirculation sending released material upwind from the release location.

Figure 16: SW winds direction. Continuous release. Plume at 10, 500 and 1000 seconds.

Figure 17 shows the plume for the five releases at 10, 500 and 1000 seconds with the WNW wind. The lateral dispersion of this plume is narrower compared to the case of the SW wind. There is also a large recirculation in front of the Two Penn Plaza building that sends released material upwind from the release location. Some released material was channeled through Broadway Avenue.

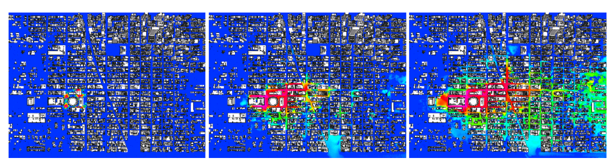

Figure 17: WNW winds direction. Continuous release. Plume at 10, 500 and 1000 seconds.

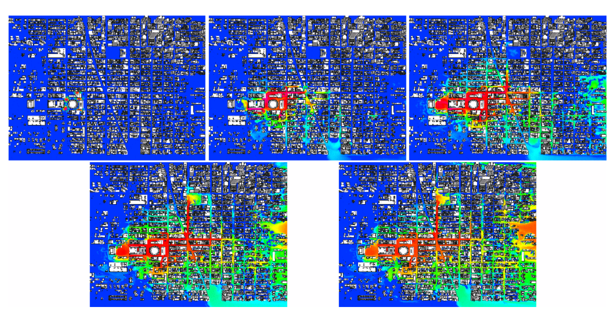

Figure 18: WNW winds direction. Puff release.

Plume at 10, 500, 1000, 2000 and 3000 seconds.

An instantaneous release was simulated for the WNW wind condition. In this simulation the same five sources of the continuous release were used. The duration of this instantaneous release was of 300 seconds. Figure 18 shows the plume for the five releases at 10, 500 and 1000 seconds with WNW wind. The two first snapshots (10 and 500 seconds) are very similar to the ones for the continuous release (Figure 17). The snapshot that corresponds to 1000 seconds shows how the level of concentration starts to decrease in the far right end of the image.

The footprint of the plumes for the continuous releases with SW and WNW winds show very different dispersion rates in the lateral direction respect to the main wind direction. A large lateral dispersion on the SW wind direction is observed if is compared with the lateral dispersion of the WNW wind direction release. This augmentation in the lateral dispersion is due to the street orientation respect to the wind direction. If the wind is aligned with the streets (WNW wind direction), the lateral dispersion is not as large as in the case of a tilt of the streets orientations and wind direction (SW wind direction).

5. CONCLUSION

FEFLO-URBAN has been successfully tested and validated against problems of atmospheric dispersion for the past 10 years. The use of CFD tools has proved to be useful in the process of design planning for experiments (MSG05). The embedded grid approach greatly reduced the man hours expended to build the geometry of the MSG area. The FEFLO-URBAN simulation results of the MSG were part of preliminary studies for the MSG05 Tracer experiment, conducted in March, 2005. The use of CFD to study the possible scenarios previous to a field experiment was proved to be a success for the MSG tracer experiment. The knowledge of different plume footprints helped the distribution of resources on the ground. These series of simulations showed the effects of tall buildings (chimney effect) and the important relation between wind direction and street orientation for the lateral dispersion of the release material. Further simulations are been conducted for the second stage of the New York experiment. The final goal of this study is to compare the several CFD results among them and with the experimental data obtained during this field campaign.

6. REFERENCES

Alessandrini, B., and G. Delhommeau, 1996: A multigrid velocity-pressure-free surface elevation fully coupled solver for calculation of turbulent incompressible flow around a hull. *Proc. 21st Symposium on Naval Hydrodynamics*.

Bell, J. B., and D. L. Marcus, 1992: A second order projection method for variable density flows. *J. Comput. Phys.*, **101**.

Bell, J. B., P. Colella, and H. Glaz, 1989: A second order projection method for the Navier-Stokes equations. *J. Comput. Phys.*, **85,** 257-283.

Camelli, F., and R. Löhner, 2000a: Flow and dispersion around buildings: an application with FEFLO. *Proc. for ECCOMAS 2000, European Congress on Computational Methods*.

——, 2000b: Reproducing Prairie Grass experiment with CFD techniques. *4th Annual George Mason University Transport and Dispersion Modeling Workshop*.

Camelli, F., S. R. Hanna, and R. Löhner, 2004a: Simulation of the MUST field experiment using the FEFLO-Urban CFD model. *Fifth Symposium on the Urban Environment*, Vancouver, Canada, AMS.

Camelli, F., R. Löhner, W. C. Sandberg, and R. Ramamurti, 2004b: VLES study of ship stack gas dynamics. *AIAA Paper 2004-0072*.

Eaton, E., 2001: Aero-acoustic in an Automotive HVAC Module. *American PAM User Conf.*, Birmingham, Michigan.

Hanna, S. R., S. Tehranian, B. Carissimo, R. W. Macdonald, and R. Löhner, 2002: Comparisons of model simulations with observations of mean flow and turbulence within simple obstacle arrays. *Atmos. Environ.*, **36,** 5067-5079.

Kallinderis, Y., and A. Chen, 1996: An incompressible 3-D Navier-Stokes method with adaptive hybrid grids. *AIAA Paper 1996-0293*.

Karbon, K. J., and R. Singh, 2002: Simulation and Design of Automobile Sunroof Buffeting Noise Control. *8th AIAA-CEAS Aero-Acoustics Conf.*, Breckenridge.

Kim, J., and P. Moin, 1985: Application of a fractional-step method to incompressible Navier-Stokes equations. *J. Comput. Phys.*, **59,** 308-323.

Löhner, R., 1990: A fast finite element solver for incompressible flows. *AIAA Paper 1990-0398*.

——, 2004: Multistage explicit advective prediction for projection-type incompressible flow solvers. *J. Comput. Phys.*, **195,** 143-152.

Löhner, R., C. Yang, E. Oñate, and S. Idelssohn, 1999: An unstructured grid-based parallel free surface solver. *Appl. Numer. Math.*

Löhner, R., J. D. Baum, E. Mestreau, D. Sharov, C. Charman, and D. Pelessone, 2004: Adaptive embedded unstructured grid methods.

International Journal of Numerical Methods in Engineering, **60,** 641-660.
Ramamurti, R., and R. Löhner, 1996: A parallel implicit incompressible flow solver using unstructured meshes. *Comput. Fluids*, **5,** 119-132.
Smagorinsky, J., 1963: General circulation experiments with the primitive equations. **I**: the basic experiment. *Mon. Wea. Rev.*, **91,** 99-165.